Molecular Therapy
Methods & Clinical Development
Original Article

Preclinical Evaluation of a Cell-Based Gene Therapy Using the Sleeping Beauty Transposon System in Choroidal Neovascularization

Maria Hernandez,[1,2,15] Sergio Recalde,[1,2,15] Laura Garcia-Garcia,[1,2,15] Jaione Bezunartea,[1] Csaba Miskey,[3] Sandra Johnen,[4] Sabine Diarra,[4] Attila Sebe,[3] Juan Roberto Rodriguez-Madoz,[5] Severine Pouillot,[6] Corinne Marie,[7,13] Zsuzsanna Izsvák,[8,9] Daniel Scherman,[7] Martina Kropp,[10,11] Felipe Prosper,[5,12] Gabriele Thumann,[10,11] Zoltán Ivics,[3] Alfredo Garcia-Layana,[1,2,14] and Patricia Fernandez-Robredo[1,2,14]

[1]Experimental Ophthalmology Laboratory, Ophthalmology, Clínica Universidad de Navarra, IdiSNA, Pamplona, Spain; [2]Red Temática de Investigación Cooperativa Sanitaria en Enfermedades Oculares, Oftared, ISCIII, Madrid, Spain; [3]Division of Medical Biotechnology, Paul Ehrlich-Institut, 63225 Langen, Germany; [4]Department of Ophthalmology, University Hospital RWTH Aachen, 52074 Aachen, Germany; [5]Regenerative Medicine Program, Center for Applied Medical Research (CIMA), University of Navarra, IdiSNA, Pamplona 31008, Spain; [6]GenoSafe, Evry 91000, France; [7]Université de Paris, UTCBS, CNRS, INSERM, F-75006 Paris, France; [8]Max Delbrück Center for Molecular Medicine in the Helmholtz Association, Berlin, Germany; [9]Berlin Institute of Health, Berlin, Germany; [10]Experimental Ophthalmology, University of Geneva, 1205 Geneva, Switzerland; [11]Department of Ophthalmology, University Hospitals of Geneva, 1205 Geneva, Switzerland; [12]Area of Cell Therapy, Clínica Universidad de Navarra, University of Navarra, IdiSNA, Pamplona 31008, Spain; [13]Chimie ParisTech, PSL Research University, F-75005 Paris, France

Age-related macular degeneration (AMD) is a progressive retinal disorder characterized by imbalanced pro- and antiangiogenic signals. The aim of this study was to evaluate the effect of *ex vivo* cell-based gene therapy with stable expression of human pigment epithelium-derived factor (PEDF) release using the non-viral *Sleeping Beauty* (*SB100X*) transposon system delivered by miniplasmids free of antibiotic resistance markers (pFAR4). Retinal pigment epithelial (RPE) cells and iris pigment epithelial (IPE) cells were co-transfected with pFAR4-inverted terminal repeats (ITRs) CMV-PEDF-BGH and pFAR4-CMV-*SB100X*-SV40 plasmids. Laser-induced choroidal neovascularization (CNV) was performed in rats, and transfected primary cells (transfected RPE [tRPE] and transfected IPE [tIPE] cells) were injected into the subretinal space. The leakage and CNV areas, vascular endothelial growth factor (VEGF), PEDF protein expression, metalloproteinases 2 and 9 (MMP-2/9), and microglial/macrophage markers were measured. Injection with tRPE/IPE cells significantly reduced the leakage area at 7 and 14 days and the CNV area at 7 days. There was a significant increase in PEDF and the PEDF/VEGF ratio with tRPE cells and a reduction in the MMP-2 activity. Our data demonstrated that *ex vivo* non-viral gene therapy reduces CNV and could be an effective and safe therapeutic option for angiogenic retinal diseases.

INTRODUCTION

Choroidal neovascularization (CNV) occurs mainly as a consequence of the imbalance between pro and antiangiogenic factors, such as vascular endothelial growth factor (VEGF) and pigment epithelium-derived factor (PEDF), respectively.[1,2] This imbalance is the hallmark of several retinal pathologies including the neovascular form of age-related macular degeneration (AMD), high myopia,[3] and proliferative diabetic retinopathy.[4] AMD is the leading cause of irreversible severe vision loss and legal blindness in adults over 55 years of age in developed countries.[5–7] It is estimated that 196 million individuals will be affected with AMD by 2020, which is a health and social problem, especially for the elderly population.[8,9]

Currently, there is no cure for AMD, and the therapy for the neovascular form is focused at controlling the CNV on inhibiting VEGF levels by disrupting the angiogenic cascade by frequent (almost monthly) intravitreal injections of anti-VEGF antibodies, which have considerable costs,[10,11] thereby representing a serious public health issue.[12] Repeated doses of anti-VEGFs are usually needed for several years, because cessation may result in the recurrence of CNV.[13] Although VEGF antagonists have been shown to be safe,[14] side effects mainly related to the injection have been detected.[15] Moreover, given that VEGF is an essential factor for cell survival,[16] it has been suggested that repeated exposure to VEGF antagonists may damage retinal neurons.[17,18] Therefore, novel strategies are developed aiming to achieve an antiangiogenic status by means other

Received 3 September 2019; accepted 30 October 2019;
https://doi.org/10.1016/j.omtm.2019.10.013.

[14]Senior author

[15]These authors contributed equally to this work.

Correspondence: Maria Hernandez, Experimental Ophthalmology Laboratory, Ophthalmology, Clínica Universidad de Navarra, IdiSNA, Pamplona, Spain.
E-mail: mahersan@unav.es
Correspondence: Patricia Fernandez-Robredo, Experimental Ophthalmology Laboratory, Ophthalmology, Clínica Universidad de Navarra, IdiSNA, Pamplona, Spain.
E-mail: pfrobredo@unav.es

than blocking VEGF to inhibit CNV and, at the same time, by avoiding repeated injections.

Because reduction of PEDF levels is linked to the pathogenesis of neovascular AMD, PEDF treatment is beneficial to treat this degenerative disorder. Exogenously administered PEDF provides potent antiangiogenic activity by directly inhibiting proliferation of endothelial cells and/or inducing their death through both extrinsic and intrinsic apoptotic pathways.[1,2,19] PEDF has demonstrated to have anti-inflammatory properties, by decreasing the expression of pro-inflammatory factors such as the tumor necrosis factor-α (TNF-α) as shown in a rat model of retinopathy.[20] In addition, PEDF also exhibits antioxidant properties, as well as broad neurotrophic effects.[21–23]

However, the half-life of PEDF is 6 h, and thus even shorter than currently used anti-VEGF molecules,[24] which makes it incapable of offering an alternative to currently required repeated injections. In order to solve the problems generated by the requirement of frequent injections, due to the transient expression of the therapeutic PEDF, several strategies are currently in development for reducing treatment burden. These include antiangiogenic gene therapies with adeno-associated viruses (AAVs), small-molecule drugs, facilitating higher concentrations and potentially longer duration than current anti-VEGF agents, and sustained-release anti-VEGF delivery systems such as the ranibizumab Port Delivery System, GB-102, NT-503, hydrogel depot, Durasert, and ENV1305.[25]

Alternatively, we pursue a gene therapy approach based on non-viral gene delivery of the antiangiogenic PEDF into cells isolated from the eye by the integrating *Sleeping Beauty* (*SB*) transposon system (recently reviewed by Narayanavari et al.,[26] Kebriaei et al.,[27] Hodge et al.[28] Hudecek et al.,[29] and Hudecek and Ivics[30]). In a previous pilot study, we observed that transplantation of *SB*-engineered rat retinal pigment epithelial (rRPE) cells and rat iris pigment epithelial (rIPE) cells expressing PEDF seemed to reduce the development of new vessels by almost 50% in a rat model of CNV.[31] Although the time window available to study changes after RPE and IPE cell transplantations is limited using the laser-induced CNV model,[32–34] this model is highly suitable to study short-term angiogenesis, inflammation, and proteolysis biomarkers. In the present study we investigated the efficacy of the hyperactive *SB100X* transposase combined with pFAR4 miniplasmids to transfect primary IPE or RPE cells at two different doses to continuously release human PEDF (hPEDF) in an established model of CNV in rats. We also aimed at determining insertion sites and exploring histologically and biochemically morphological alterations related to the angiogenic status after transplantation of genetically modified primary cells secreting human antiangiogenic PEDF.

RESULTS

Localization of Transplanted Venus-Transfected Cells in the Subretinal Space

First, we addressed whether genetic engineering of RPE and IPE cells would compromise their biological properties. Using phase-contrast microscopy, no changes in either cell morphology or pigmentation were observed in rRPE (Figure S1A) and rIPE cells cultured *ex vivo* (Figure S1F). Venus expression was observed after transfection with pFAR4-inverted terminal repeats (ITRs)-CAGGS Venus plasmid in rRPE cells (Figures S1B–S1D) and rIPE cells (Figures 1G–1I). Cultured rRPE cells were positive for RPE65 (Figure S1E) and rIPE cells for CK18 antibodies (Figure S1J). Following transplantation into the subretinal space of experimental rats, automated digital (Figures 1A and 1B) and confocal microscope (Figures 1C–1N) were used to confirm the localization and survival of transfected RPE (tRPE) and transfected IPE (tIPE) cells expressing the Venus fluorescent reporter protein at 1 week post-injection. To confirm that the Venus cells were the injected ones, we labeled transfected cells with CellBrite (a plasmatic membrane marker) before injection (Figures 1G–1N). We observed that SB-engineered cells maintained their cellular properties and identity, and survived *in vivo* following transplantation in the eye.

PEDF and VEGF Release by *SB*-Engineered Rat Primary RPE and IPE Cells

Having established the basic parameters for gene delivery with the *SB* transposon system, we addressed the biological properties of rRPE and rIPE cells engineered with the hPEDF following transplantation into the eyes of rats that had previously undergone laser-induced triggering of CNV. To confirm that the PEDF detected was produced by the plasmids (hPEDF), the pFAR4/ITRs CMV-PEDF-BGH and pFAR4/ITRs CMV-PEDF-histidine (His)-BGH miniplasmids were used to transfect the rat cells alongside with a source of the *SB100X* transposase. Before injection into the subretinal space, the primary cells were transfected with the construct pFAR4-ITRs CMV PEDF-His BGH plasmid in order to identify the transplanted cells with PEDF and His tag. We detected engineered PEDF-His reporter-expressing RPE and IPE cells using anti-PEDF (mouse monoclonal, MAB1059, 1:1,000; Chemicon) and anti-His antibodies (6-His, goat polyclonal, NBP1-25939, 1:400; Novus, Cambridge, UK) (Figures 2A–2E). Moreover, retinal homogenates showed that gene expression of rat PEDF (rPEDF) mRNA was similar in saline and the RPE-PEDF-SB groups as expected (Figure 2F), although gene expression of rPEDF mRNA in IPE cells showed a significant increase in the 5,000 tIPE-PEDF-SB group versus saline (Figure 2G) ($p < 0.05$). Specific hPEDF mRNA was detectable only in tRPE/tIPE-PEDF-SB cells and not in the saline-treated control group. The hPEDF increase was highly significant in the 10,000 PEDF-SB group ($p < 0.001$) versus all injected eyes in tRPE cell and tIPE cell groups compared with saline (Figures 2H and 2I).

At the protein level, PEDF expression was significantly increased in animals injected with 10,000 tRPE-PEDF-SB cells versus the saline group (Figure 3A) ($p < 0.05$). However, no significant differences were found in the tIPE-PEDF-SB and IPE-PEDF groups (Figure 3B). Notably, rVEGF protein expression level was similar in the injected tRPE/IPE-PEDF-SB and tRPE/IPE-PEDF animals (Figures 3C and 3D). Importantly, as a consequence of PEDF release by the engineered cells, the antiangiogenic ratio (PEDF/VEGF) was significantly

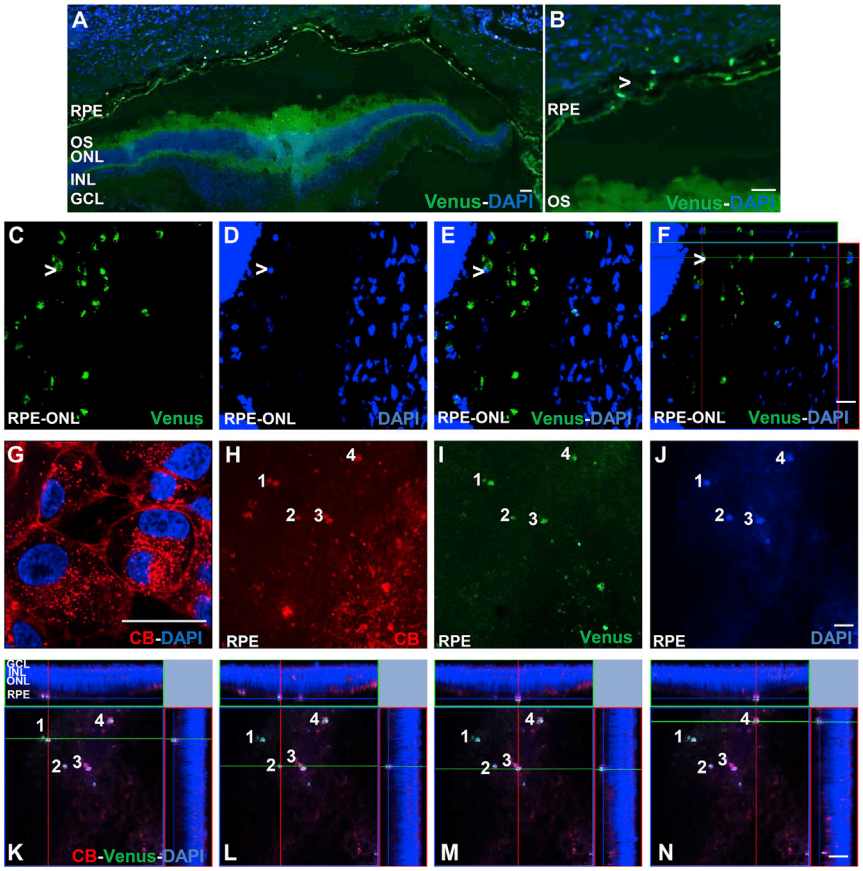

Figure 1. Fluorescence Representative Images of Rat Primary Cells in the Subretinal Space after Injection

(A) An automatic mosaic image of Venus-RPE cells (green) in the rat subretinal space. (B) Detail of a group of Venus-RPE cells in the RPE. (C–F) Confocal images of Venus-RPE cells in subretinal area between RPE and ONL. (C and D) Cells were transfected with the pFAR4-ITRs-CAGGS Venus miniplasmid (green), and the nuclei were stained with DAPI (blue). (E) Merged image from (C) and (D). (F) Orthogonal projection of the injected Venus cells. Arrows indicate Venus primary cells injected. (G) RPE cells labeled with CellBrite (red) and DAPI (blue) in a super-resolution image captured. (H–N) Confocal images of a group of Venus-CellBrite-RPE cells in the subretinal space near the RPE. Four RPE cells are represented (H–J) with their orthogonal projection confocal images (K–N). Nuclei are labeled with DAPI (blue). Scale bars: (A–F) 100 μm, (G) 20 μm, (H–N) 50 μm. CB, CellBrite; GCL, ganglion cell layer; INL, inner nuclear layer; ONL, outer nuclear layer; OS, outer segment; PEDF, pigment epithelium-derived factor; RPE, retinal pigment epithelium.

increased in 10,000 tRPE-PEDF-SB animals (Figure 3E) ($p < 0.05$) versus the Saline group, whereas in the remaining groups no significant changes were observed (Figure 3F). These data suggested that, as a result of shifting the antiangiogenic ratio, PEDF-expressing cells could affect angiogenesis and neovascularization.

Matrix metalloproteinase-2 (MMP-2) plays an important role in the formation of new blood vessels and in endothelial cell migration, a key feature of angiogenesis.[35–37] Additionally, MMP-9 has also been suggested to play a complex, indirect role in angiogenesis by promoting VEGF mobilization.[38] Importantly, previous studies have indicated that MMPs play important roles in early AMD.[35,39] Disequilibrium of the gelatinases suggests a role of abnormal extracellular matrix metabolism that breaks through the basal membrane into the sub-retinal space. Active MMP-2 and MMP-9 can induce the proteolysis of PEDF in the extracellular matrix of the cell and thus interfere with the antiangiogenic and neurotrophic activities of the cellular PEDF protein.[40–43] We found that MMP-2 activity levels were significantly lower in eyes of rats injected with 10,000 RPE-PEDF-SB cells versus the saline group (Figure 3G) ($p < 0.05$), whereas no differences were observed in the IPE-PEDF-SB and IPE-PEDF groups (Figure 3H). In addition, MMP-9 activity levels were similar in all groups injected with RPE or IPE cells (Figures 3I and 3J).

Antiangiogenic Effects Elicited by SB-Engineered Rat Primary IPE and RPE Cells Expressing hPEDF

In order to assess the effect of the hPEDF release on vascular leakage, we used fluorescein angiography (FA) at 7 and 14 days post-laser treatment. We did not observe a decrease in the percentage of the leakage area in animals injected with tRPE cells at 7 days (Figures 4A and 4C); however, a statistically significant decrease of the leakage area was observed at day 7 in the 10,000 tIPE-PEDF-SB group versus animals injected with saline ($p < 0.01$; Figures 4B and 4D). Fourteen days post-laser treatment, animals injected with 5,000 and 10,000 tRPE-PEDF-SB cells showed a statistically significant decrease in the area of the fluorescein leakage (Figures 4E and 4G) ($p < 0.01$). Similarly, animals injected with 10,000 tIPE-PEDF-SB cells showed a significant decrease in FA area (Figures 4F and 4H) ($p < 0.01$).

We measured the most important indicator of antiangiogenic effects, the CNV areas at 7 and 14 days post-laser treatment, and a statistically significant decrease in the percentage of CNV area in the 5,000 ($p < 0.05$) and 10,000 tRPE-PEDF-SB groups ($p < 0.01$) and in the 10,000 tRPE-PEDF group ($p < 0.05$) at the 7-day time point (Figures 4I and 4J) was observed. In IPE cells, we observed a statistically significant CNV area decrease in the 10,000 tIPE-PEDF-SB and 10,000 tIPE-PEDF groups (Figures 4K and 4L) ($p < 0.05$). These results indicate that PEDF-engineered cells can elicit a measurable antiangiogenic effect. This effect is especially pronounced in animals injected with 10,000 tRPE-PEDF-SB cells, which also displayed the highest ratio of PEDF over VEGF protein expression (Figures 3A and 3E). The CNV area decreased in all experimental groups analyzed at 14 days post-laser (with the exception of the 10,000 tRPE-PEDF group), but

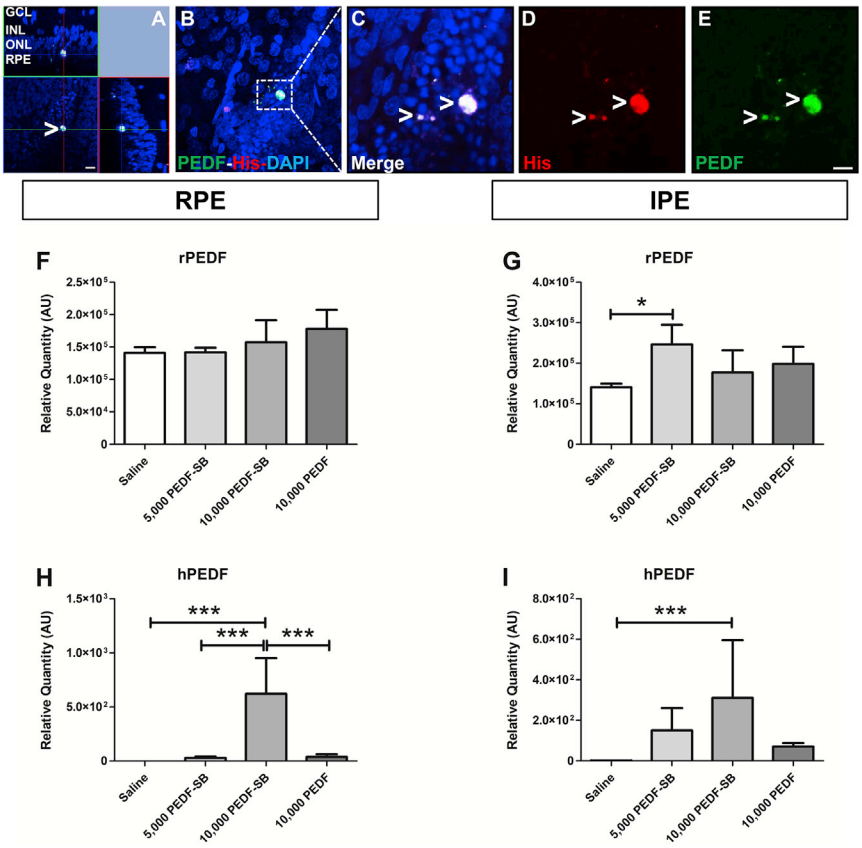

Figure 2. Results of the rPEDF and hPEDF Determination in Retinas Injected with tRPE and tIPE Cells with PEDF-His and *SB100X* Plasmid

(A–E) Representative immunofluorescence images of the tRPE cells colocalized with anti-His (red) and anti-hPEDF (green) antibodies. (A) Orthogonal projection of RPE cells localized between RPE and ONL. (B–E) RPE cells immunostained with PEDF and His in detail at super-resolution confocal microscopy. Arrows indicate the cell group observed. DAPI (blue)-labeled nuclei. Scale bar: 50 μm. (F) No changes in the expression of rPEDF mRNA in RPE cells. (G) Expression of hPEDF mRNA in IPE cells with a significant increase in the 5,000 IPE-PEDF-SB group versus saline-injected eye. (H and I) Expression of hPEDF mRNA in RPE-PEDF-SB cells (H) and IPE-PEDF-SB cells (I). The increase of the hPEDF was significantly high in the 10,000 RPE/IPE-PEDF-SB group versus all groups in RPE cells ($p < 0.001$) and versus saline-injected eye in IPE cells ($p < 0.001$). Data are presented as mean ± SEM ($n = 4$) (*$p < 0.05$, ***$p < 0.001$). AU, arbitrary units; GCL, ganglion cell layer; His, histidine; hPEDF, human pigment epithelium-derived factor; INL, inner nuclear layer; ONL, outer nuclear layer; PEDF, pigment epithelium-derived factor; RPE, retinal pigment epithelium; rPEDF, rat pigment epithelium-derived factor.

those differences did not reach statistical significance (Figures 4M–4P). This result is consistent with the known limitations of this CNV model.[32]

The specific Iba1 and CD68 markers are expressed in activated microglia and macrophages, respectively, in tissues with inflammation,[36] whereas apoptotic cells are caspase-3 positive. Anatomical observations and fluorescence quantification following transplantation at days 7 and 14 indicated that microglial activation (Iba1) and macrophage infiltration (CD68) were not statistically different in rats injected with tRPE/IPE-PEDF-SB and tRPE/IPE-PEDF groups (Figures S3A–S3D; Figures 5A–5D). After 14 days post-laser treatment, we observed an increase in Iba1 and CD68 expression in animals transplanted with 5,000 and 10,000 RPE-PEDF-SB (Figures 5C and 5E) and IPE-PEDF-SB cells (Figures 5D and 5F); however, this increase was not statistically significant. At 7 and 14 days after laser photocoagulation, no changes in caspase-3-positive cells were found in the outer nuclear layer (ONL) of injection-treated retinas versus saline-injected eye (Figures S3E–S3H).

Close-to-Random Profile of *SB*-Mediated Transgene Integration in rRPE and rIPE Cells

Insertions of therapeutic foreign DNA into the genome are subject to position effects, which may alter cell physiology and lead to malignant transformations. Consistent with the results obtained in other cell types,[37,44,45] the *SB* transposon system exhibits a close-to-random profile of genomic integration in therapeutically relevant human T cells[46–48] and $CD34^+$ hematopoietic stem and progenitor cells (HSPCs).[49,50]

In order to assess the relative safety of *SB* transposon-mediated gene delivery in the context of the here described *in vivo* AMD gene therapy model, we analyzed the genome-wide insertion profiles of PEDF transgene-bearing *SB* vectors in rRPE and rIPE cells. At the primary DNA sequence level, TA dinucleotides positioned at the center of an 8-bp palindromic AT repeat, a canonical molecular signature of *SB* chromosomal integration,[47] were found to be the preferred sites of *SB* integration in rat cells (Figure 6A). In agreement with earlier findings, we found that *SB* insertions show only a minor bias toward actively transcribed genes and a depletion in exon sequences and 5′ UTRs (Figure 6B). As in other cell types, we found a slight correlation between insertion frequencies and the relative transcriptional activities at the insertion sites (Figure S4).

Integration of therapeutic gene constructs into genomic "safe harbors" (GSHs) in the human genome would prevent insertional mutagenesis and associated risks of oncogenesis in gene therapy. GSHs are regions of the human genome that support predictable expression of newly integrated DNA without adverse effects on the host cell. GSHs can be bioinformatically allocated to chromosomal sites or regions if they satisfy the following criteria: (1) distance of at least 50 kb from

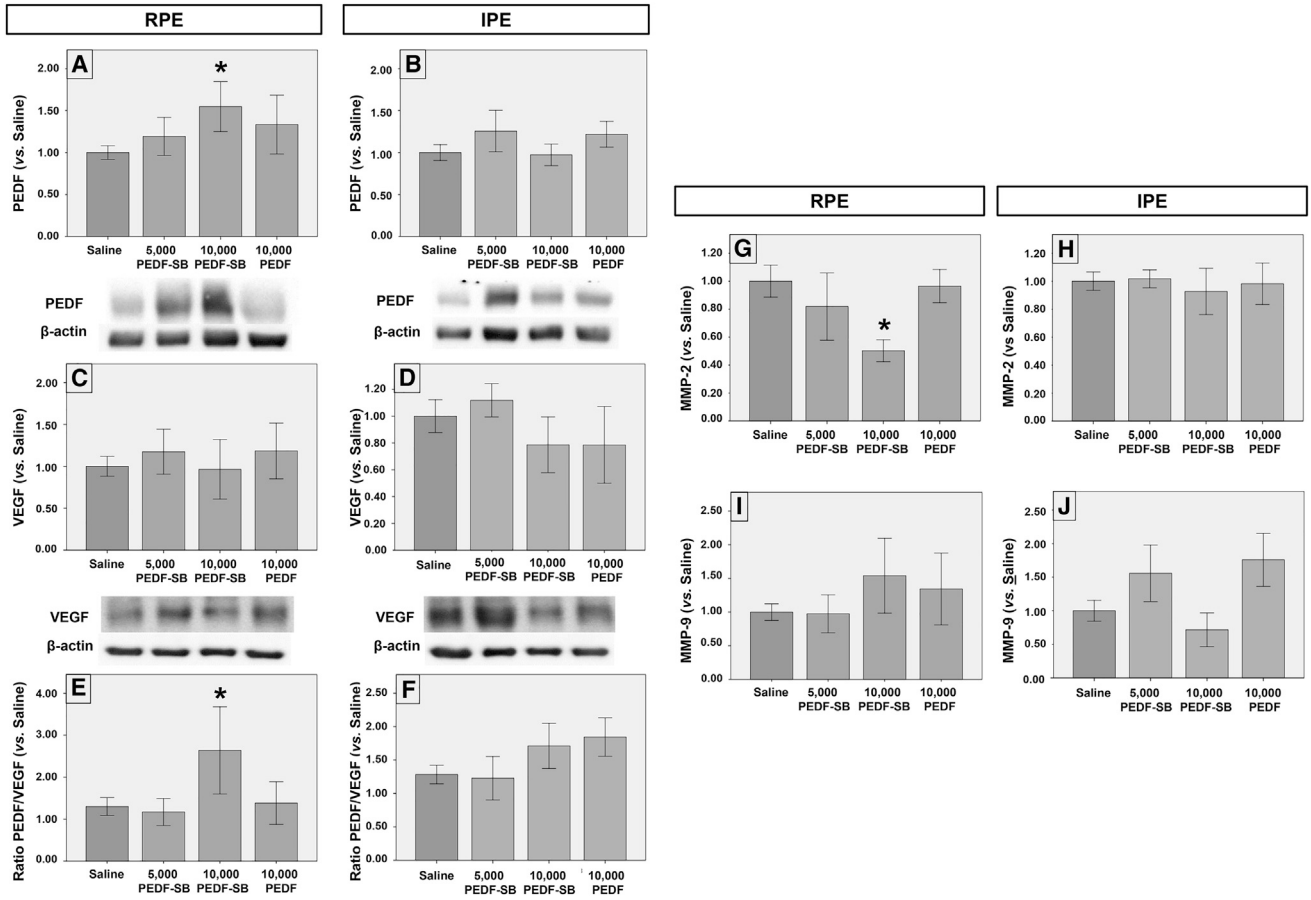

Figure 3. Analysis of PEDF, VEGF, PEDF/VEGF Ratio, and MMP-2 and -9 Activity Analysis

(A–F) PEDF (A and B) and VEGF (C and D) expression in rats injected with tRPE (A, C, and E) and IPE (tIPE) cells (B, D, and F) (5,000 and 10,000 PEDF-SB and 10,000 PEDF cells) versus saline injection. PEDF and VEGF expression ratio (E and F) in rats injected with tRPE (E) and tIPE (F) cells (5,000 and 10,000 PEDF-SB and 10,000 PEDF cells) versus saline injection. (G–J) MMP-2 (G and H) and MMP-9 (I and J) activity in homogenates from rat eyes injected with tRPE (G and I) and IPE (tIPE) cells (H and J) (5,000 and 10,000 PEDF-SB and 10,000 PEDF cells) versus saline injection. PEDF expression (A) and PEDF/VEGF ratio (E) were significantly increased in rats injected with RPE-10,000 PEDF-SB, whereas no changes in VEGF expression were observed. MMP-2 expression was significantly decreased in rats injected with RPE-10,000 PEDF-SB (G), whereas no changes in MMP-9 were observed. Data are presented as percentage of AU mean ± SEM (n = 5) (*$p < 0.05$ versus Saline). AU, arbitrary units; MMP, metalloproteinase; PEDF, pigment epithelium-derived factor; tIPE, transfected iris pigment epithelial (cells); tRPE, transfected retinal pigment epithelial (cells); VEGF, vascular endothelial growth factor.

the 5′ end of any gene; (2) distance of at least 300 kb from any cancer-related gene (see above); (3) distance of at least 300 kb from any microRNA (miRNA) gene; (4) location outside transcription units; and (5) location outside ultra-conserved regions (UCRs) of the rat genome.[47,51] The *SB* insertion sites in rat retinal cells occur at GSHs at a frequency of 33% (Figure 6C), which was in line with previous observations in human T cells,[48] HSPCs, as well as human RPE cells.[49,50] Collectively, our analysis on vector biosafety predicts a favorable transgene insertion profile of *SB* for therapeutic gene transfer in RPE and IPE cells.

DISCUSSION

Here we demonstrate that transplantation of genetically modified RPE and IPE cells using pFAR4 plasmids encoding the *SB100X* transposase overexpressing PEDF prevents and suppresses vessel leakage and CNV, and regenerates the natural VEGF/PEDF balance. The main features that define the severity of the retinal pathology include vessel leakage, CNV area, and a proangiogenic environment. Leakage is an indicator of the high permeability and immaturity of vessels that leak fluid and blood, thus provoking edema, hemorrhages, and finally, loss of vision.[52] The CNV area defines the severity of the disease, which is dependent on the proangiogenic state of the surrounding environment. Importantly, alongside the elevated PEDF level, a decrease of MMP-2 expression is according to the observed antiangiogenic environment following tIPE and tRPE cell therapy. These results are consistent with our previous pilot studies showing safety, effectiveness at a higher single dose, and survival of PEDF-expressing cells transplanted in the rat subretinal space.[31,49,53–58]

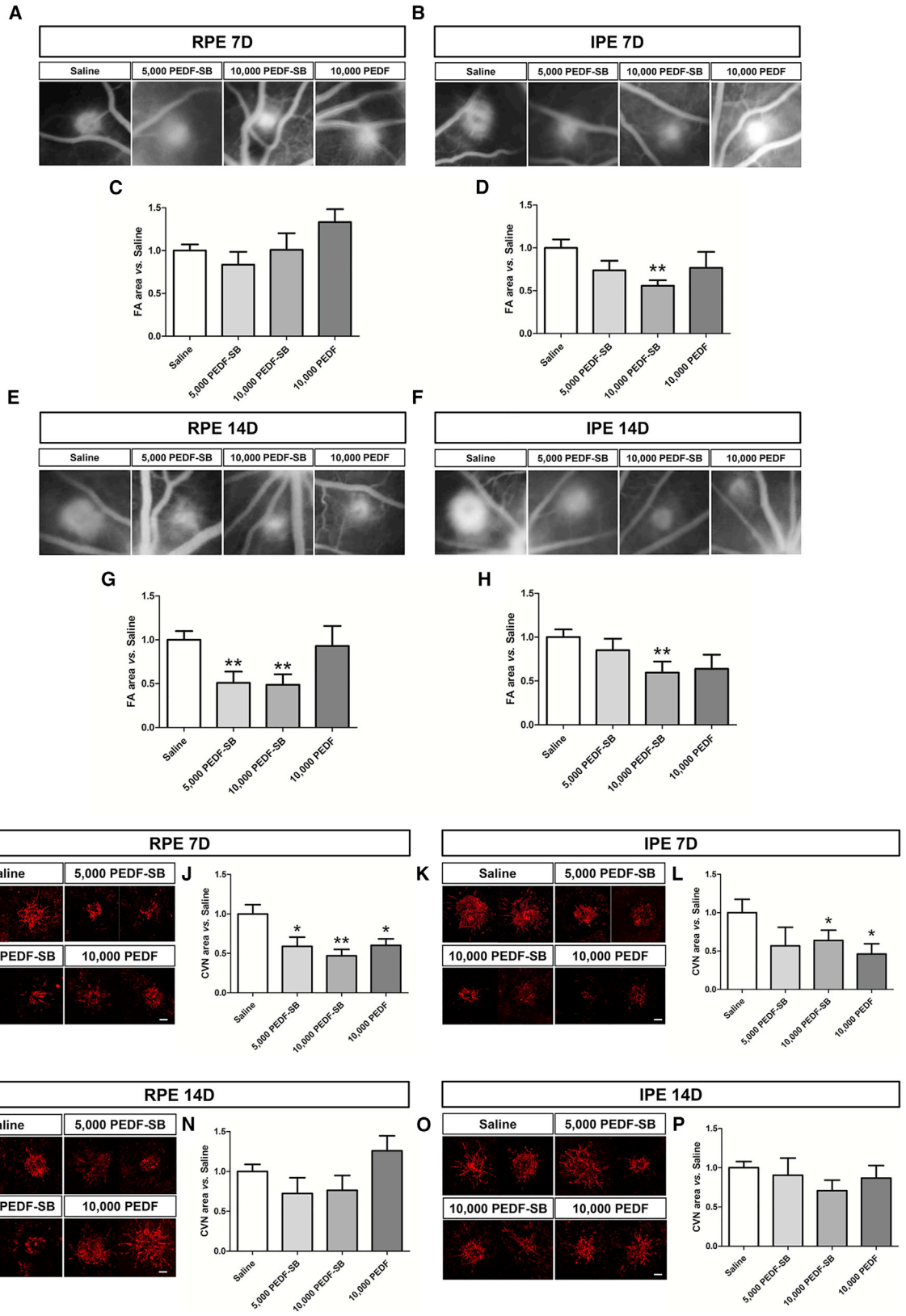

(legend on next page)

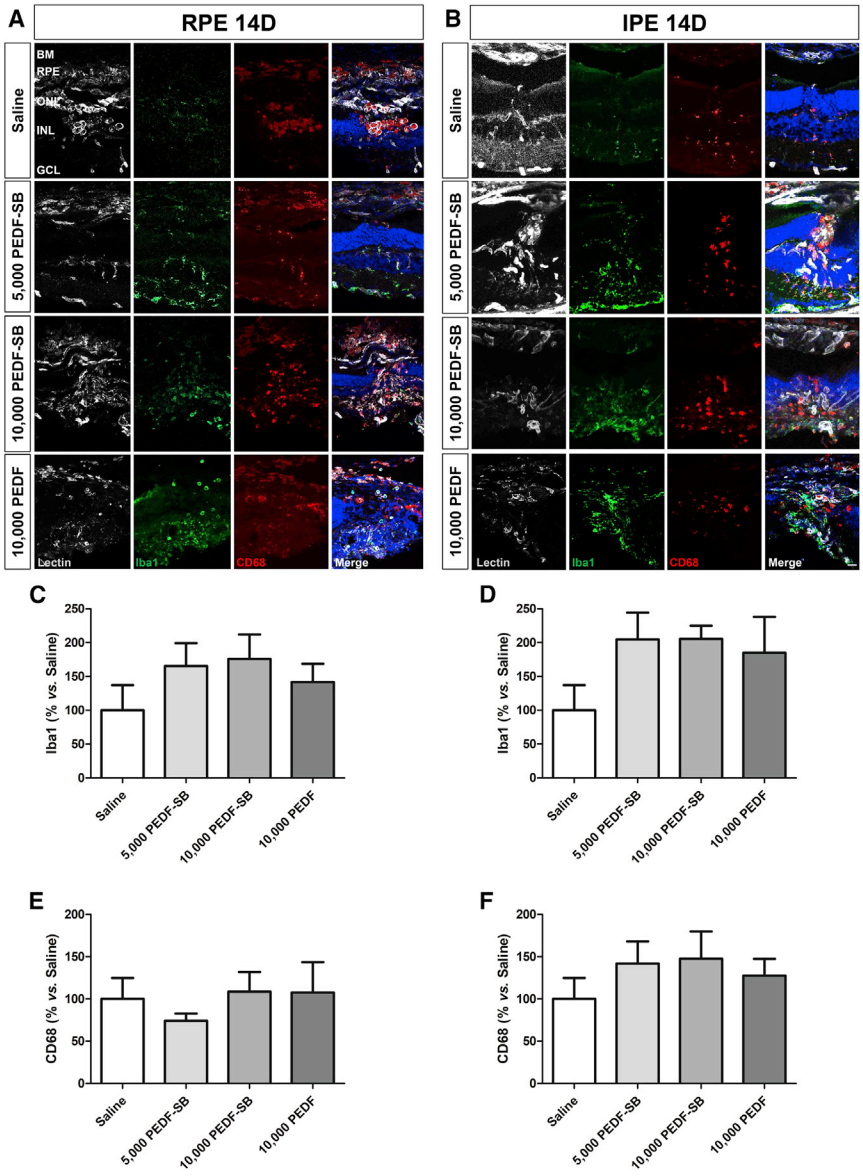

Figure 5. Iba1 and CD68 Expression Immunofluorescence Images in CNV Areas 14 Days after Laser in Rats Injected with tRPE and tIPE Cells

(A–F) Immunofluorescence retinal images (A and B) and intensity measurements (C–F) of lectin (gray), Iba1 (green), and CD68 (red) in rats injected with tRPE (A, C, and E) and tIPE (B, D, and F) cells (5,000 and 10,000 PEDF-SB and 10,000 PEDF cells) versus saline injection after 14 days post-laser. Nuclei are labeled with DAPI (blue). Data are presented as percentage mean ± SEM (n = 4). Scale bar: 100 μm. BM, Bruch's membrane; GCL, ganglion cell layer; INL, inner nuclear layer; ONL, outer nuclear layer; PEDF, pigment epithelium-derived factor; RPE, retinal pigment epithelium; tIPE, transfected iris pigment epithelial (cells); tRPE, transfected retinal pigment epithelial (cells).

described for the self-replicating episomal vector pEPito. This alternative, non-viral vehicle has been shown to efficiently deliver an expression vector for PEDF for the treatment of diabetic retinopathy in a mouse model.[59] Second, although both doses of PEDF-expressing cells were effective in our experiments, mainly the higher dose (10,000 cells) was able to significantly reduce (1) FA leakage, (2) CNV area, and (3) MMP-2 activity. Thus, higher doses of therapeutic cells may be superior for a sustained benefit, likely because they are more potent to generate an antiangiogenic environment in the retina by shifting the balance between pro and antiangiogenic factors (e.g., VEGF and PEDF).

The role of PEDF in macrophage recruitment is largely unknown, and we found no changes in macrophage infiltration, active microglia, and early apoptosis after laser-induced CNV. Cell transplantation induced no significant change in microglia activation at 7 and 14 days post-laser, but was slightly increased in all groups analyzed versus the saline group at 14 days postinjection. This accumulation of subretinal and retinal microglia was in turn associated with multiple features reminiscent of AMD histopathology, including local RPE structural changes and CNV formation.[60–62] Microglia activation could be due to PEDF release, because PEDF activates microglial metabolism without stimulation and proliferation in cell culture

The experimental data allow us to draw two important conclusions with respect to applying a cell-based gene therapy approach to AMD. First, transposase-mediated permanent insertion of the PEDF transgene is effective in reducing CNV, and sustained expression of PEDF might be a likely key to elicit therapeutically relevant effects in the context of AMD. This correlates well to what was

Figure 4. Fluorescence Angiography (FA), Analyses of the Leakage Area Lectin Staining in Four CNV Areas per Flatmounts, and Analysis of the CNV Measurements in All Groups Studied

(A–H) FA images (A, B, E, and F) and measurement of the percentage leakage area (C, D, G, and H) at 7 (A–D) and 14 days (E–H) post-laser in rats injected with tRPE (A, C, E, and G) and tIPE cells (B, D, F, and H) (5,000 and 10,000 PEDF-SB and 10,000 PEDF cells) versus saline injection. (I–P) Fluorescence lectin-stained images (I, K, M, and O) and measurement of the CNV area (J, L, N, and P) at 7 (I–L) and 14 days (M–P) post-laser in rats injected with tRPE (A, B, E, and F) and tIPE cells (C, D, G, and H) (5,000 and 10,000 PEDF-SB and 10,000 PEDF cells) versus saline injection. Data are presented as percentage mean ± SEM (n = 6) (**$p < 0.01$, *$p < 0.05$ versus Saline). Scale bars: 100 μm. PEDF, pigment epithelium-derived factor; tIPE, transfected iris pigment epithelial (cells); tRPE, transfected retinal pigment epithelial (cells).

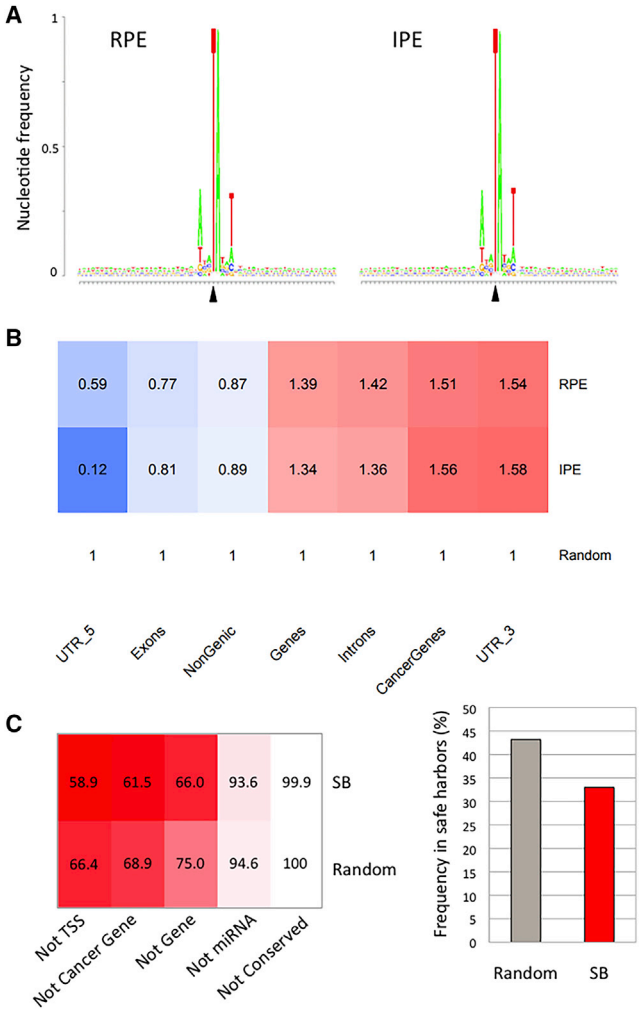

Figure 6. Genome-wide Distribution of hPEDF Transgene-Containing *Sleeping Beauty* Transposons in rRPE and IPE Cells

(A) Sequence logo representing consensus sequences of *SB* integration sites. The logo displays the canonical TA integration sites (marked with arrowheads) embedded in an AT-rich local sequence environment. (B) Distribution of *SB* insertions in functional genomic segments. Color intensities depict the degree of deviation (red for enrichment and blue for depletion) from the expected random distribution, which was set to 1. (C) Representation of vector insertion sites corresponding to genomic safe harbor criteria. The numbers represent percent values of all insertions of the corresponding group. Color intensities imply deviation from an ideal, 100% representation. On the right, the overall frequencies of SB insertion sites (in red) and random expected frequencies (in gray) in GSHs are shown. IPE, iris pigment epithelial (cells); PEDF, pigment epithelium-derived factor; RPE, retinal pigment epithelial (cells).

experiments.[60] Moreover, a minor activation of microglia also occurs in human induced pluripotent stem cell (hiPSC)-derived RPE allografts without signs of rejection/toxicity.[63]

Several preclinical studies over the last few years have made an effort to transplant RPE cells derived from human embryonic stem cells (hESCs) in minipigs[64,65] and rabbits,[66] RPE cells derived from iPSCs in monkeys,[63,67] human fetal RPE xenografts in monkeys,[68] and RPE suspension cells and IPE xenotransplant in The Royal College of Surgeons (RCS) rats.[69–71] The transplanted cells in those studies maintained local tissue integrity, because cells were found to be well tolerated in clusters in the subretinal space, and no signs of rejection were observed for relatively long periods of time from 1 to 6 months. However, clinical applications of hESC- and hiPSC-derived cells still need to solve technical limitations and safety barriers, such as genetic and phenotypic variations, risk of graft rejection due to immune response, or cancer formation.[63,72] In the case of AMD patients, transplanted RPE-choroid sheets and RPE/IPE cell suspensions were non-toxic and appeared to survive.[73–75] Recently, two multidisciplinary clinical trials have reported preliminary results with RPE derived from hESCs on a synthetic membrane for dry AMD[76] and wet AMD[77] treatment. Both research groups tested subretinal implants, and the preliminary results indicated that hESC-derived RPE implants are safe, at least in the short-term, and may be a feasible treatment for AMD.

Building upon research targeting PEDF as a therapeutic factor for AMD, a number of studies involving gene and cell therapy are being pursued. Success of PEDF delivery using non-integrating adenoviral vectors has been limited[78] because of the short duration of gene expression and the adverse effects associated with traditional gene delivery techniques.[79–81] As a consequence, there is a great demand for developing a treatment that allows for the maintenance of high PEDF level for an extended period of time. In Europe, a phase Ib/IIa *ex vivo* gene therapy clinical trial for long-term expression of PEDF in IPE cells by combining pFAR4 miniplasmid and *SB* transposon technologies is planned and has been submitted for approval to Swiss regulatory authorities Swissmedic[31,49,55] (https://www.targetamd.eu/), with all preclinical tests completed.[82] Our approach is based on the use of RPE and IPE cells because they show similar characteristics and many functions in common. RPE cells express PEDF and secrete it into the interphotoreceptor matrix, where it exerts its neurotrophic, antiinflammatory, and antiangiogenic activity.[83] Moreover, other studies have demonstrated that IPE cells of vertebrates are able to maintain an exceptional plasticity for cell-replacement therapy in many retinal diseases (reviewed by Thumann[84]), and by CNV inhibition in rats and preventing the death of photoreceptor cells in the RCS rat model.[85] In addition, IPE cells can replace lost or damaged RPE in the macular area of AMD patients.[74,86–88] The *in vitro* and transplantation studies suggest that IPE cells possess a dormant potential to redifferentiate into a different phenotype[89–91] and may acquire RPE functionality in the subretinal environment. Given the limitations to obtain RPE and IPE cells in humans associated to the surgery for the future treatment, we transfected both types of cells with different densities, 5,000 and 10,000 cells. Surgical iridectomy to isolate IPE cells is a relatively straightforward procedure and a non-invasive intervention in patients.[92]

The advantages of using the non-viral *SB* system include its ability to support sustained long-term expression of the therapeutic gene, its relatively safe genome-wide insertion profile, associated with the lower

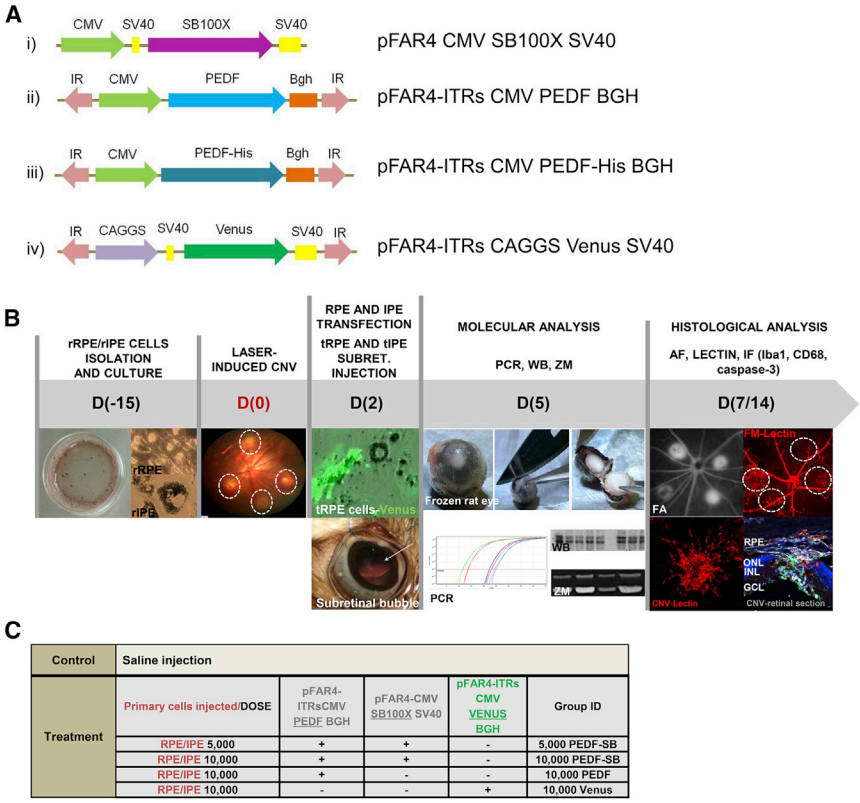

Figure 7. Diagram of the Plasmids Used in the Study and Timeline

(A) Schematic diagram of the various constructs used in the study: (i) pFAR4 CMV SB100X SV40 plasmid, (ii) pFAR4-ITRs CMV PEDF BGH plasmid, (iii) pFAR4-ITRs CMV PEDF-His BGH plasmid, and (iv) pFAR4-ITRs CAGGS Venus SV40 plasmid. (B) Timing and experimental procedures developed. (C) Animal groups, treatments (cell type, doses, and plasmid), and nomenclature used in the study. CNV, choroidal neovascularization; D, day; FA, fluorescein angiography; FM, flatmount; GCL, ganglion cell layer; Iba-1, anti-ionized calcium-binding adaptor molecule 1; INL, inner nuclear layer; ONL, outer nuclear layer; PEDF, pigment epithelium-derived factor; rIPE, rat iris pigment epithelial (cells); rRPE, rat retinal pigmented epithelial (cells); tIPE, transfected iris pigment epithelial (cells); tRPE, transfected retinal pigmented epithelial (cells); WB, western blot; ZM, zymography.

regulatory burden, and significantly reduced costs of the GMP vector manufacturing.[30] Plasmids are easier and cheaper to produce, ship, and store.[93] In contrast, gammaretroviral and lentiviral vectors commonly utilized in gene therapy tend to integrate in a non-random manner. Preferential integrations of gammaretroviral vectors near transcriptional regulatory elements of active genes[94,95] and of lentiviral vectors based toward bodies of genes[95] bear an increased genotoxicity risk already manifested in patients treated with gammaretroviral vectors by leukemogenesis during early gene therapy clinical trials.[96] A fairly random profile of *SB* integrations may offer a safer alternative for lifelong genetic correction of therapeutically relevant cell types, including RPE and IPE cells. Further potential advantages of a gene therapy approach for AMD probably include the simplicity and reduced costs because of the dispensation of lifelong reinjections of the anti-VEGFs in patients. Therefore, either alone or combined with anti-VEGF therapy, the present cell-based non-viral *SB100X*-mediated PEDF gene therapy can be considered for AMD patients as a novel therapy, especially in the field of personalized medicine.

MATERIALS AND METHODS

Vector Components, Construction, and Production of pFAR4 Miniplasmids

Construction of the PEDF transposon plasmid, whose expression cassette contains the hPEDF gene flanked by *SB* transposon ITRs, and stable gene delivery using the hyperactive *SB100X* transposase system have been previously reported.[31,49,54,55] The schematic diagram of the plasmids and constructs used in the study were shown in Figure 7A.

Isolation, Cultivation of Rat Primary IPE and RPE Cells, and Transfection of RPE and IPE Cells

The study was performed according to the Association for Research in Vision and Ophthalmology (ARVO) Resolution on the Use of Animals in Ophthalmic and Vision Research and approved by the Ethics Committee for Animal Research of the University of Navarra (protocol approval number 023-13).

Brown Norway male rats (8–15 weeks old; Charles River Laboratories, Wilmington, MA, USA) were used to isolate and cultivate RPE and IPE cells (n = 45) according to the technical protocol used by Garcia-Garcia et al.[31] Prior to use of the cells for transfection, a RPE/IPE sample was cultured on coverslips for phenotyping confirmation by immunofluorescence (Figures S1A–S1J). All transfections were carried out by electroporation with the Neon Transfection System using the 10 μL Kit (Thermo Fisher Scientific) following the manufacturer's protocol. Electroporation parameters for primary cells were 1,100 V, 20 ms, and 2 pulses. In order to verify the transfection, cells were transfected with pFAR4-ITRs-CAGGS Venus plasmid, and tRPE and tIPE cells were observed and photographed by the inverted microscope (Leica, Microsystems CMS, Wetzlar, Germany) (Figures S1C, S1D, S1H, and S1I). tRPE and tIPE cells with different plasmids were directly injected after transfection (Figure 7B).

Laser-Induced CNV Model and Subretinal Injection

Adult Brown Norway rats (Charles River, Wilmington, MA, USA) were housed in standard cages with 12-h light/dark cycle and food and water provided *ad libitum*. Animals were anesthetized with a mixture of ketamine (75 mg/kg; Imalgene 1000; Merial Laboratories, Barcelona, Spain) and xylazine (10 mg/kg; Xilagesic 2%; Calier

Laboratories, Barcelona, Spain), and eyes were dilated with a mixture of phenylephrine (7.8 mg/mL; Alcon Cusí, Barcelona, Spain) and tropicamide (3 mg/mL; Alcon Cusí) eye drops. CNV lesions were created by using an 810-nm diode laser (Oculight SLx; Iridex, Buckinghamshire, UK). Four laser photocoagulation spots (250 mW intensity, 0.05 s, and 75-μm spot size) were placed concentrically around the optic nerve using a coverslip as a contact lens. Eyes that were assigned to undergo molecular analyses gene expression, western blot analysis, and zymographies received 12 laser applications. Rupture of Bruch's membrane was confirmed by bubble formation. Laser rupture sites with hemorrhage or subretinal bleeding at the time of laser application were excluded from analysis.[32]

For subretinal injection, rats were intraperitoneally anesthetized with a mixture of ketamine and xylazine as previously mentioned to minimize animal suffering. Before transfection of cells, supernatants were subjected to mycoplasma analysis using the Mycoplasma Detection Kit (13100-01; Southern Biotech, Birmingham, AL, USA). Only after a negative result, cells were transfected and suspended in PBS at the appropriate density to inject the number of cells needed in 5 μL. Pupils were dilated and double-anesthetic (tetracaine chlorhydrate 1 mg/10 mL and oxybuprocaine chlorhydrate 4 mg/10 mL; Alcon cusí) eye drops were used to anesthetize the eyes. In brief, eyes were stabilized using a suture, and the superior conjunctiva and subconjunctival tissues were cut to expose the sclera. A hole was made into the subretinal space using a 27G needle where the cells were injected using a 25G de Juan cannula (Synergetics, O'Fallon, MO, USA) attached to a 25-μL Hamilton syringe (Hamilton Messtchnik, Höchst, Germany). No suture was placed, and oxytetracycline (Terramicina; Farmasierra Laboratories, Madrid, Spain) antibiotic was applied. To evaluate the efficacy of the treatment, 2 days after inducing CNV, 5,000 and 10,000 IPE or RPE cells were transfected with the pFAR4-ITRs CMV-PEDF-BGH miniplasmid with and without the *SB100X* transposase (pFAR4-CMV SB100X SV40) (Figure 7C), ratio 16:1 in a total plasmid concentration of 0.5 μg DNA. After proper tip positioning, ascertained by a focal whitening of the retina, an equivalent of 5,000 or 10,000 cells (50 μL of cell suspension) was injected subretinally below the optic nerve head. Animals were euthanized at 7 and 14 days after injection (n = 6). Saline injection was used as the control group. The experimental design and groups studied were identified in Figures 7B and 7C.

FA

At 7 and 14 days after laser coagulation, FA images were generated on anesthetized rats after intraperitoneal injection of 10% fluorescein sodium. After photocoagulation, subretinal injection was confirmed by identifying retinal bubble formation as previously reported by our group.[31] Images were captured using a digital camera (Topcon TRC 50FX camera; Topcon Corporation, Tokyo, Japan). Leaking fluorescein may result from incompetent blood vessels as visible in CNV or through a diseased RPE that no longer blocks fluorescein leakage originating from the choroid. Areas of leakage in an FA show gradual enlargement and blurring of their margins.[97] The leakage area (in pixels) was measured using ImageJ software (NIH, Bethesda, MD, USA) by two blinded, independent, trained, and experienced observers. Mean leakage area was calculated for each study group as previously described,[31,32] and differences between treated and control animals were assessed.

RNA Isolation and Quantitative Real-Time PCR

To determine the expression of hPEDF and rPEDF mRNA in the treated eyes, we performed a PCR analysis in retinas transplanted with 10,000 tRPE/tIPE-PEDF-SB cells. At 5 days post-laser, animals were sacrificed for molecular analyses. The quantitative real-time PCRs (n = 3 per study group) were performed in cryogenic eye cups of anesthetized rats. The posterior pole (including the whole retina with RPE) was placed in 200 μL Lysis buffer (RNeasy Kit; QIAGEN, Hilden, Germany) in a reaction tube, immediately homogenized by pipetting up and down in a sterile pipette tip for 20 times, and stored at −20°C until RNA isolation. RNA isolation was performed according to the recommendations of the manufacturer (RNASPIN MINI., 25-0500-71; GE Healthcare, Chicago, IL, USA). RNA was eluted in RNase-free water (20 μL) and stored at −80°C. The cDNA synthesis was done using Qscript cDNA Quanta BIO protocol for reverse transcription (QIAGEN). The cDNA was diluted to a concentration of 1,000 ng/μL, corresponding to the initially measured total RNA. hPEDF, rat VEGF, and rPEDF mRNAs were quantified in eyes of rats using the RTqPCR 7300 system (Applied Biosystem, Foster City, CA, USA) and Applied Biosystems gene expression assays (Hs01106934_m1, Rn01511601_m1, and Rn00709999_m1, respectively). Relative quantity of each mRNA was calculated for hPEDF and rPEDF or rVEGF threshold cycle (Ct) normalized to Ct of Ribosomal Protein L30 (RPL30) (Rn00821148_g1) and multiplied by 1E+5 for an easier representation. The results have been determined with the Relative Quantification software from Applied Biosystems v.1.2 after analysis of each qPCR plate with the SDS v.2.3 software.

Zymography of MMP-2 and MMP-9

Standard methodology for gelatin zymography was used to detect MMP activity in eye homogenates samples of animals injected with tRPE and tIPE cells with or without *SB100X* as described previously.[32,98] The MMP activation ratio for MMP-2 was calculated as active MMP intensity/active MMP + proMMP intensity. The MMP-9 activity was also determined using intensity measurements. Each zymography assay was repeated at least three times to ensure accuracy.

Western Blotting for VEGF and PEDF

Five micrograms of eye homogenates samples was mixed with Laemmli buffer (Bio-Rad, CA, USA), boiled for 5 min, separated on 10%–12% SDS-PAGE gels, and transferred to a nitrocellulose membrane. After blocking with 5% skimmed milk (w/v), 0.1% Tween 20 (w/v) in TBS (1 h, room temperature [RT]), membranes were exposed to a rat monoclonal anti-VEGF antibody (1:5,000, 512808; BioLegend, San Diego, CA, USA) at RT for 1 h followed by incubation at RT for 1 h with a horseradish peroxidase (HRP)-conjugated goat anti-rat immunoglobulin G (IgG)-peroxidase-conjugated antibody (1:5,000, 31470; Pierce Biotechnology, Waltham, MA, USA).

Membranes were tested for monoclonal anti-PEDF (1:1,000; MAB1059; Millipore, Burlington, MA, USA) overnight at 4°C followed by incubation at RT for 2 h with a goat anti-mouse IgG-HRP (1:10,000; sc2005; Santa Cruz Biotechnology, Dallas, TX, USA). Signals were detected with an enhanced chemiluminescence (ECL) kit (ECL western blotting detection kit; GE Healthcare) and captured with ImageQuant 400 (GE Healthcare). The relative intensities of the immunoreactive bands were analyzed with ImageQuantTL software (GE Healthcare). The loading was verified by Ponceau S red (Sigma-Aldrich, St. Louis, MO, USA), and the same blot was stripped and reblotted with an anti-β-actin monoclonal antibody (Sigma-Aldrich) to normalize the VEGF and PEDF levels.

Choroidal Flatmounts and Neovascularization

Brown Norway rats (n = 6 per study group) were euthanized at 7 and 14 days post-laser. Eyes were enucleated and fixed for 1 h in 4% paraformaldehyde diluted in PBS at 4°C. RPE-choroid-sclera complexes were microsurgically isolated and incubated with blocking buffer containing PBS, 3% Triton X-100, 0.5% Tween 20, 2% sodium azide, and 1% FBS for 1 h at 4°C. Then, they were incubated with biotinylated isolectin (GS-IB4; Vector Labs, Burlingame, CA, USA) overnight at RT, and the flatmounts were washed in PBS and incubated in Alexa Fluor Streptavidin 594 (1:250; S32356; Life Technologies, Carlsbad, CA, USA). The CNV lesions were captured under a confocal microscope (LSM800; Zeiss, Oberkochen, Germany), and the areas were measured by Fiji ImageJ software.

Immunofluorescence of Frozen Sections

The eyes of Brown Norway rats (n = 3) were enucleated and fixed for 1 h in 4% paraformaldehyde diluted in phosphate buffer (PB) at 4°C. After incubation, the eyes were washed in PBS and cryoprotected in 30% sucrose solution for 24 h. The tissues were embedded in OCT compound (Tissue-Tek-Sakura, Leiden, the Netherlands) and stored at −20°C. The eyeballs were cut into cross sections at 12–14 μm with a cryostat (Microm HM550; Thermo Fisher Scientific) and stored at −80°C until used.

Three to four retinal sections of the area of neovascularization per group were chosen. The frozen sections were fixed with 4% paraformaldehyde and a 0.3 M glycine solution for 5 min to prevent detachment of the section from the slides. Then, the sections were blocked with blocking buffer solution as mentioned above. Antibodies for the triple staining were added: anti-mouse CD68 (1:100; MCA341R; AbD Serotec, Bio-Rad), anti-ionized calcium-binding adaptor molecule 1 (Iba1), anti-goat Iba1 (1:250; ab5076; Abcam, Cambridge, UK) or anti-rabbit Iba1 (1:250; CP290A; Biocare, Berkshire, UK), and anti-rabbit caspase-3 (1:250; ab13847; Abcam), and incubated overnight at 4°C. After washing with PBS, the secondary antibodies, donkey anti-mouse Alexa Fluor 596 (1:250; A10036; Life Technologies), anti-donkey anti-goat Alexa Fluor 488 (1:250; A11055; Life Technologies), and donkey anti-rabbit Alexa Fluor 647 (1:250; A31573; Life Technologies), were added and incubated for 1 h at RT. All sections were additionally incubated with isolectin as mentioned in the flatmount labeling to visualize the neovascularization. DAPI (Sigma-Aldrich) was used as the nuclear marker. Then sections were mounted with PBS-glycerol (1:1) and analyzed under a confocal microscope (LSM800; Zeiss). Quantification of the fluorescence images was performed by ImageJ. We used the following formula to measure the total immunofluorescence intensity (TII) per CNV area image: TII = CNV (ii) − BG (ii)/HAA (ii) − BG (ii), where BG represents background, HAA represents healthy adjacent area, and ii represents immunofluorescence intensity, and compared the TII mean percentage in the CNV area between analyzed study groups. The cells immunostained with Iba1 and CD68 in CNV areas were identified in Figure S2.

Vector Insertion Site Analysis

Genomic DNA was isolated from RPE and IPE cells using the Quick DNA Kit (Zymo Research, Irvine, CA, USA). We used the procedure already described[48] with the following modifications: 1 μg of DNA per sample was sonicated with the Covaris M220 ultra-solicitor device. After end-repair, A-tailing, and linker ligation, the terminal segments of the SB transposon inverted repeats and their flanking genomic sequences were amplified in two rounds of PCR. In the first round, 6 μL of purified ligation reaction was used with 25 pmol of the primers specific for the linker and for the transposon inverted repeat, Linker and T-Bal-Long, respectively, with the following conditions: 98°C for 30 s; 10 cycles of 98°C for 10 s, 72°C for 30 s; 15 cycles of 98°C for 10 s, ramp to 62°C (1°C/s) for 30 s, 72°C for 30 s, and 72°C for 5 min. The nested PCRs performed on 5 μL of the purified first round PCR products with the PE-nest-ind-N and SB-20-bc-ill-N primers (where N is the number of the Illumina TruSeq indexes) were run with the following program: 98°C for 30 s; 15 cycles of 98°C for 10 s, ramp to 64°C (1°C/s) for 30 s, 72°C for 30 s, and 72°C for 5 min. The primer sequences have already been published.[48] After 1.5% agarose gel separation, the 300–500 bp range of the smears was column purified and sequenced on HiSeq Illumina instruments at Genewiz USA.

Bioinformatic Analysis of the Insertion Sites

The quality trimming, filtering, and mapping conditions have been described elsewhere.[48] The reads were aligned onto the rn5 rat genome using the rn5 with bowtie.[99,100] The downstream analyses were performed in the R environment[101] with homemade scripts. The composition and frequencies of the nucleotides at *SB* insertion sites of the genome were determined and plotted using the SeqLogo tool. The annotation of the insertion sites in genic features and in GSHs was done using the genomation package.[102] The random set of 10,000 theoretical insertion sites in the rat genome was generated computationally. The cancer-related genes represent the rat orthologs of the human cancer gene set downloaded from the Bushman Lab website (http://www.bushmanlab.org/links/genelists). The orthologous positions were obtained from Ensembl (http://www.ensembl.org/biomart/martview/59de4d4d3503246cb451221246ed7978). UCRs of the rat genome were arbitrarily determined from the phastCons13way track for the rn5 assembly retrieved from the University of California Santa Cruz (UCSC) table browser (http://genome.ucsc.edu/) by filtering regions with scores ≥800. Expressional data on the rat retinal

transcriptome were published by Kozhevnikova et al.[103] We used the expressional dataset obtained from the retinas of 3-month-old Wistar rats. Non-expressed genes of the retina were defined on the bases of absence of reads from the genes in the dataset. The expressed genes were grouped into five sets of the same size according their expression levels, and insertions were counted in them and compared with a random expected frequency determined with the random insertion dataset.

Statistical Analysis

Data are presented as mean ± SEM. Statistical analysis was performed using SPSS 2.0 (SPSS, Chicago, IL, USA) and GraphPad Prism 5.0 (GraphPad Software, San Diego, CA, USA) programs. *In vitro* studies were analyzed applying an ANOVA for repeated measures. For CNV area results, one-way ANOVA was followed by Bonferroni post hoc tests for multiple comparisons after confirming normal distribution of the data. $p < 0.05$ was considered statistically significant.

SUPPLEMENTAL INFORMATION

Supplemental Information can be found online at https://doi.org/10.1016/j.omtm.2019.10.013.

AUTHOR CONTRIBUTIONS

Conceptualization: P.F.-R., A.G.-L., F.P., M.H., S.R., L.G.-G.; Data Curation: L.G.-G., M.H., J.B., S.R., P.F.-R., C. Miskey; Funding Acquisition: G.T., A.G.-L., P.F.-R., D.S., Z. Izsvák, Z. Ivics, F.P., S.J.; Investigation: L.G.-G., S.R., M.H., J.B., P.F.-R., M.K.; Methodology: S.D., M.K., C. Miskey, C. Marie, A.S., J.B., J.R.R.-M., S.P.; Resources: Z. Izsvák, Z. Ivics, D.S., C. Marie; Supervision: A.G.-L., P.F.-R., F.P., G.T., D.S., Z. Ivics, Z. Izsvák.; Writing – Original Draft: L.G.-G., S.R., M.H., P.F.-R.; Writing – Review & Editing: M.H., S.R., G.T., A.G.-L., P.F.-R., D.S., Z. Izsvák, Z. Ivics, F.P., S.J., C. Miskey, C. Marie.

CONFLICTS OF INTEREST

A.G.-L. is a consultant for Thea, Allergan, Bayer, Novartis, and Roche Laboratories. Z. Izsvák and Z. Ivics are co-inventors on several patents on *Sleeping Beauty* transposon technology.

ACKNOWLEDGMENTS

This work was supported by the European Union's Seventh Framework Programme for research, technological development, and demonstration (grant agreement no. 305134) and Fundación Jesús Gangoiti Barrera. Publication costs have been financed by Fundación Multiópticas (Spain) within a collaborative project with the University of Navarra. L.G.-G. received a predoctoral grant from the Asociación de Amigos de la Universidad de Navarra, Spain. Z. Izsvák was funded by European Research Council, ERC Advanced [ERC-2011-ADG 294742].

REFERENCES

1. Folkman, J., and Ingber, D. (1992). Inhibition of angiogenesis. Semin. Cancer Biol. *3*, 89–96.
2. Das, A., and McGuire, P.G. (2003). Retinal and choroidal angiogenesis: pathophysiology and strategies for inhibition. Prog. Retin. Eye Res. *22*, 721–748.
3. Ohno-Matsui, K., Ito, M., and Tokoro, T. (1996). Subretinal bleeding without choroidal neovascularization in pathologic myopia. A sign of new lacquer crack formation. Retina *16*, 196–202.
4. Askou, A.L. (2014). Development of gene therapy for treatment of age-related macular degeneration. Acta Ophthalmol. *92* (Thesis3), 1–38.
5. Klein, R., Cruickshanks, K.J., Nash, S.D., Krantz, E.M., Nieto, F.J., Huang, G.H., Pankow, J.S., and Klein, B. (2010). The prevalence of age-related macular degeneration and associated risk factors. Arch. Ophthalmol *128*, 750–758.
6. Klein, R., Klein, B.E.K., and Linton, K.L.P. (1992). Prevalence of age-related maculopathy. The Beaver Dam Eye Study. Ophthalmology *99*, 933–943.
7. Mehta, S. (2015). Age-Related Macular Degeneration. Prim. Care *42*, 377–391.
8. Wong, W.L., Su, X., Li, X., Cheung, C.M.G., Klein, R., Cheng, C.-Y., and Wong, T.Y. (2014). Global prevalence of age-related macular degeneration and disease burden projection for 2020 and 2040: a systematic review and meta-analysis. Lancet Glob. Health *2*, e106–e116.
9. Bourne, R.R.A., Flaxman, S.R., Braithwaite, T., Cicinelli, M.V., Das, A., Jonas, J.B., Keeffe, J., Kempen, J.H., Leasher, J., Limburg, H., et al.; Vision Loss Expert Group (2017). Magnitude, temporal trends, and projections of the global prevalence of blindness and distance and near vision impairment: a systematic review and meta-analysis. Lancet Glob. Health *5*, e888–e897.
10. Chakravarthy, U., Harding, S.P., Rogers, C.A., Downes, S.M., Lotery, A.J., Wordsworth, S., and Reeves, B.C.; IVAN Study Investigators (2012). Ranibizumab versus bevacizumab to treat neovascular age-related macular degeneration: one-year findings from the IVAN randomized trial. Ophthalmology *119*, 1399–1411.
11. Martin, D.F., Maguire, M.G., Fine, S.L., Ying, G.S., Jaffe, G.J., Grunwald, J.E., Toth, C., Redford, M., and Ferris, F.L., 3rd; Comparison of Age-related Macular Degeneration Treatments Trials (CATT) Research Group (2012). Ranibizumab and bevacizumab for treatment of neovascular age-related macular degeneration: two-year results. Ophthalmology *119*, 1388–1398.
12. Hollingworth, W., Jones, T., Reeves, B.C., and Peto, T. (2017). A longitudinal study to assess the frequency and cost of antivascular endothelial therapy, and inequalities in access, in England between 2005 and 2015. BMJ Open *7*, e018289.
13. Klettner, A., Tahmaz, N., Dithmer, M., Richert, E., and Roider, J. (2014). Effects of aflibercept on primary RPE cells: toxicity, wound healing, uptake and phagocytosis. Br. J. Ophthalmol. *98*, 1448–1452.
14. Saenz-de-Viteri, M., Fernández-Robredo, P., Hernández, M., Bezunartea, J., Reiter, N., Recalde, S., and García-Layana, A. (2016). Single- and repeated-dose toxicity study of bevacizumab, ranibizumab, and aflibercept in ARPE-19 cells under normal and oxidative stress conditions. Biochem. Pharmacol. *103*, 129–139.
15. Lois, N., McBain, V., Abdelkader, E., Scott, N.W., and Kumari, R. (2013). Retinal pigment epithelial atrophy in patients with exudative age-related macular degeneration undergoing anti-vascular endothelial growth factor therapy. Retina *33*, 13–22.
16. Carmeliet, P., De Smet, F., Loges, S., and Mazzone, M. (2009). Branching morphogenesis and antiangiogenesis candidates: tip cells lead the way. Nat. Rev. Clin. Oncol. *6*, 315–326.
17. Saint-Geniez, M., Maharaj, A.S.R., Walshe, T.E., Tucker, B.A., Sekiyama, E., Kurihara, T., Darland, D.C., Young, M.J., and D'Amore, P.A. (2008). Endogenous VEGF is required for visual function: evidence for a survival role on müller cells and photoreceptors. PLoS One *3*, e3554.
18. Brar, V.S., Sharma, R.K., Murthy, R.K., and Chalam, K.V. (2010). Bevacizumab neutralizes the protective effect of vascular endothelial growth factor on retinal ganglion cells. Mol. Vis. *16*, 1848–1853.
19. Falero-Perez, J., Park, S., Sorenson, C.M., and Sheibani, N. (2017). PEDF expression affects retinal endothelial cell proangiogenic properties through alterations in cell adhesive mechanisms. Am. J. Physiol. Cell Physiol. *313*, C405–C420.
20. Zhang, S.X., Wang, J.J., Gao, G., Parke, K., and Ma, J.X. (2006). Pigment epithelium-derived factor downregulates vascular endothelial growth factor (VEGF) expression and inhibits VEGF-VEGF receptor 2 binding in diabetic retinopathy. J. Mol. Endocrinol. *37*, 1–12.
21. Tombran-Tink, J., and Barnstable, C.J. (2003). PEDF: a multifaceted neurotrophic factor. Nat. Rev. Neurosci. *4*, 628–636.

22. Tombran-Tink, J., Chader, G.G., and Johnson, L.V. (1991). PEDF: a pigment epithelium-derived factor with potent neuronal differentiative activity. Exp. Eye Res. *53*, 411–414.

23. Ek, E.T.H., Dass, C.R., and Choong, P.F. (2006). Pigment epithelium-derived factor: a multimodal tumor inhibitor. Mol. Cancer Ther. *5*, 1641–1646.

24. Amaral, J., Fariss, R.N., Campos, M.M., Robison, W.G., Jr., Kim, H., Lutz, R., and Becerra, S.P. (2005). Transscleral-RPE permeability of PEDF and ovalbumin proteins: implications for subconjunctival protein delivery. Invest. Ophthalmol. Vis. Sci. *46*, 4383–4392.

25. Hussain, R.M., and Ciulla, T.A. (2017). Emerging vascular endothelial growth factor antagonists to treat neovascular age-related macular degeneration. Expert Opin. Emerg. Drugs *22*, 235–246.

26. Narayanavari, S.A., Chilkunda, S.S., Ivics, Z., and Izsvák, Z. (2017). Sleeping Beauty transposition: from biology to applications. Crit. Rev. Biochem. Mol. Biol. *52*, 18–44.

27. Kebriaei, P., Izsvák, Z., Narayanavari, S.A., Singh, H., and Ivics, Z. (2017). Gene Therapy with the Sleeping Beauty Transposon System. Trends Genet. *33*, 852–870.

28. Hodge, R., Narayanavari, S.A., Izsvák, Z., and Ivics, Z. (2017). Wide Awake and Ready to Move: 20 Years of Non-Viral Therapeutic Genome Engineering with the Sleeping Beauty Transposon System. Hum. Gene Ther. *28*, 842–855.

29. Hudecek, M., Izsvák, Z., Johnen, S., Renner, M., Thumann, G., and Ivics, Z. (2017). Going non-viral: the Sleeping Beauty transposon system breaks on through to the clinical side. Crit. Rev. Biochem. Mol. Biol. *52*, 355–380.

30. Hudecek, M., and Ivics, Z. (2018). Non-viral therapeutic cell engineering with the Sleeping Beauty transposon system. Curr. Opin. Genet. Dev. *52*, 100–108.

31. Garcia-Garcia, L., Recalde, S., Hernandez, M., Bezunartea, J., Rodriguez-Madoz, J.R., Johnen, S., Diarra, S., Marie, C., Izsvák, Z., Ivics, Z., et al. (2017). Long-Term PEDF Release in Rat Iris and Retinal Epithelial Cells after Sleeping Beauty Transposon-Mediated Gene Delivery. Mol. Ther. Nucleic Acids *9*, 1–11.

32. Ivanescu, A.A., Fernández-Robredo, P., Heras-Mulero, H., Sádaba-Echarri, L.M., García-García, L., Fernández-García, V., Moreno-Orduna, M., Redondo-Exposito, A., Recalde, S., and García-Layana, A. (2015). Modifying choroidal neovascularization development with a nutritional supplement in mice. Nutrients *7*, 5423–5442.

33. Zarranz-Ventura, J., Fernández-Robredo, P., Recalde, S., Salinas-Alamán, A., Borrás-Cuesta, F., Dotor, J., and García-Layana, A. (2013). Transforming growth factor-beta inhibition reduces progression of early choroidal neovascularization lesions in rats: P17 and P144 peptides. PLoS ONE *8*, e65434.

34. Recalde, S., Zarranz-Ventura, J., Fernández-Robredo, P., García-Gómez, P.J., Salinas-Alamán, A., Borrás-Cuesta, F., Dotor, J., and García-Layana, A. (2011). Transforming growth factor-β inhibition decreases diode laser-induced choroidal neovascularization development in rats: P17 and P144 peptides. Invest. Ophthalmol. Vis. Sci. *52*, 7090–7097.

35. Ebrahem, Q., Qi, J.H., Sugimoto, M., Ali, M., Sears, J.E., Cutler, A., Khokha, R., Vasanji, A., and Anand-Apte, B. (2011). Increased neovascularization in mice lacking tissue inhibitor of metalloproteinases-3. Invest. Ophthalmol. Vis. Sci. *52*, 6117–6123.

36. Huang, H., Parlier, R., Shen, J.K., Lutty, G.A., and Vinores, S.A. (2013). VEGF Receptor Blockade Markedly Reduces Retinal Microglia/Macrophage Infiltration into Laser-Induced CNV. PLoS One *8*, e71808.

37. Vigdal, T.J., Kaufman, C.D., Izsvák, Z., Voytas, D.F., and Ivics, Z. (2002). Common physical properties of DNA affecting target site selection of sleeping beauty and other Tc1/mariner transposable elements. J. Mol. Biol. *323*, 441–452.

38. Hollborn, M., Stathopoulos, C., Steffen, A., Wiedemann, P., Kohen, L., and Bringmann, A. (2007). Positive feedback regulation between MMP-9 and VEGF in human RPE cells. Invest. Ophthalmol. Vis. Sci. *48*, 4360–4367.

39. Jonas, J.B., Tao, Y., Neumaier, M., and Findeisen, P. (2012). Cytokine concentration in aqueous humour of eyes with exudative age-related macular degeneration. Acta Ophthalmol. *90*, e381–e388.

40. Lamoreaux, W.J., Fitzgerald, M.E., Reiner, A., Hasty, K.A., and Charles, S.T. (1998). Vascular endothelial growth factor increases release of gelatinase A and decreases release of tissue inhibitor of metalloproteinases by microvascular endothelial cells in vitro. Microvasc. Res. *55*, 29–42.

41. Burbridge, M.F., Cogé, F., Galizzi, J.P., Boutin, J.A., West, D.C., and Tucker, G.C. (2002). The role of the matrix metalloproteinases during in vitro vessel formation. Angiogenesis *5*, 215–226.

42. Wary, K.K., Thakker, G.D., Humtsoe, J.O., and Yang, J. (2003). Analysis of VEGF-responsive genes involved in the activation of endothelial cells. Mol. Cancer *2*, 25.

43. Notari, L., Miller, A., Martínez, A., Amaral, J., Ju, M., Robinson, G., Smith, L.E., and Becerra, S.P. (2005). Pigment epithelium-derived factor is a substrate for matrix metalloproteinase type 2 and type 9: implications for downregulation in hypoxia. Invest. Ophthalmol. Vis. Sci. *46*, 2736–2747.

44. Ammar, I., Gogol-Döring, A., Miskey, C., Chen, W., Cathomen, T., Izsvák, Z., and Ivics, Z. (2012). Retargeting transposon insertions by the adeno-associated virus Rep protein. Nucleic Acids Res. *40*, 6693–6712.

45. Voigt, K., Gogol-Döring, A., Miskey, C., Chen, W., Cathomen, T., Izsvák, Z., and Ivics, Z. (2012). Retargeting sleeping beauty transposon insertions by engineered zinc finger DNA-binding domains. Mol. Ther. *20*, 1852–1862.

46. Huang, X., Guo, H., Tammana, S., Jung, Y.-C., Mellgren, E., Bassi, P., Cao, Q., Tu, Z.J., Kim, Y.C., Ekker, S.C., et al. (2010). Gene transfer efficiency and genome-wide integration profiling of Sleeping Beauty, Tol2, and piggyBac transposons in human primary T cells. Mol. Ther. *18*, 1803–1813.

47. Gogol-Döring, A., Ammar, I., Gupta, S., Bunse, M., Miskey, C., Chen, W., Uckert, W., Schulz, T.F., Izsvák, Z., and Ivics, Z. (2016). Genome-wide Profiling Reveals Remarkable Parallels Between Insertion Site Selection Properties of the MLV Retrovirus and the piggyBac Transposon in Primary Human CD4(+) T Cells. Mol. Ther. *24*, 592–606.

48. Monjezi, R., Miskey, C., Gogishvili, T., Schleef, M., Schmeer, M., Einsele, H., Ivics, Z., and Hudecek, M. (2017). Enhanced CAR T-cell engineering using non-viral Sleeping Beauty transposition from minicircle vectors. Leukemia *31*, 186–194.

49. Thumann, G., Harmening, N., Prat-Souteyrand, C., Marie, C., Pastor, M., Sebe, A., Miskey, C., Hurst, L.D., Diarra, S., Kropp, M., et al. (2017). Engineering of PEDF-Expressing Primary Pigment Epithelial Cells by the SB Transposon System Delivered by pFAR4 Plasmids. Mol. Ther. Nucleic Acids *6*, 302–314.

50. Holstein, M., Mesa-Nuñez, C., Miskey, C., Almarza, E., Poletti, V., Schmeer, M., Grueso, E., Ordóñez Flores, J.C., Kobelt, D., Walther, W., et al. (2018). Efficient Non-viral Gene Delivery into Human Hematopoietic Stem Cells by Minicircle Sleeping Beauty Transposon Vectors. Mol. Ther. *26*, 1137–1153.

51. Sadelain, M., Papapetrou, E.P., and Bushman, F.D. (2011). Safe harbours for the integration of new DNA in the human genome. Nat. Rev. Cancer *12*, 51–58.

52. Grossniklaus, H.E., and Green, W.R. (2004). Choroidal neovascularization. Am. J. Ophthalmol. *137*, 496–503.

53. Izsvák, Z., and Ivics, Z. (2004). Sleeping beauty transposition: biology and applications for molecular therapy. Mol. Ther. *9*, 147–156.

54. Johnen, S., Djalali-Talab, Y., Kazanskaya, O., Möller, T., Harmening, N., Kropp, M., Izsvák, Z., Walter, P., and Thumann, G. (2015). Antiangiogenic and Neurogenic Activities of Sleeping Beauty-Mediated PEDF-Transfected RPE Cells In Vitro and In Vivo. BioMed Res. Int. *2015*, 863845.

55. Pastor, M., Johnen, S., Harmening, N., Quiviger, M., Pailloux, J., Kropp, M., Walter, P., Ivics, Z., Izsvák, Z., Thumann, G., et al. (2018). The Antibiotic-free pFAR4 Vector Paired with the Sleeping Beauty Transposon System Mediates Efficient Transgene Delivery in Human Cells. Mol. Ther. Nucleic Acids *11*, 57–67.

56. Ivics, Z., and Izsvák, Z. (2015). *Sleeping Beauty* transposition. In Mobile DNA III, N. Craig, M. Chandler, M. Gellert, A. Lambowitz, P. Rice, and S. Sandmeyer, eds. (ASM Press). https://doi.org/10.1128/microbiolspec.mdna3-0042-2014.

57. Ivics, Z., and Izsvák, Z. (2011). Nonviral gene delivery with the *sleeping beauty* transposon system. Hum. Gene Ther. *22*, 1043–1051.

58. Johnen, S., Izsvák, Z., Stöcker, M., Harmening, N., Salz, A.K., Walter, P., and Thumann, G. (2012). Sleeping Beauty transposon-mediated transfection of retinal and iris pigment epithelial cells. Invest. Ophthalmol. Vis. Sci. *53*, 4787–4796.

59. Calado, S.M., Diaz-Corrales, F., and Silva, G.A. (2016). pEPito-driven PEDF Expression Ameliorates Diabetic Retinopathy Hallmarks. Hum. Gene Ther. Methods *27*, 79–86.

60. Sugita, Y., Becerra, S.P., Chader, G.J., and Schwartz, J.P. (1997). Pigment epithelium-derived factor (PEDF) has direct effects on the metabolism and proliferation of microglia and indirect effects on astrocytes. J. Neurosci. Res. *49*, 710–718.

61. Combadière, C., Feumi, C., Raoul, W., Keller, N., Rodéro, M., Pézard, A., Lavalette, S., Houssier, M., Jonet, L., Picard, E., et al. (2007). CX3CR1-dependent subretinal microglia cell accumulation is associated with cardinal features of age-related macular degeneration. J. Clin. Invest. *117*, 2920–2928.

62. Tuo, J., Bojanowski, C.M., Zhou, M., Shen, D., Ross, R.J., Rosenberg, K.I., Cameron, D.J., Yin, C., Kowalak, J.A., Zhuang, Z., et al. (2007). Murine ccl2/cx3cr1 deficiency results in retinal lesions mimicking human age-related macular degeneration. Invest. Ophthalmol. Vis. Sci. *48*, 3827–3836.

63. Sugita, S., Iwasaki, Y., Makabe, K., Kamao, H., Mandai, M., Shiina, T., Ogasawara, K., Hirami, Y., Kurimoto, Y., and Takahashi, M. (2016). Successful Transplantation of Retinal Pigment Epithelial Cells from MHC Homozygote iPSCs in MHC-Matched Models. Stem Cell Reports *7*, 635–648.

64. Koss, M.J., Falabella, P., Stefanini, F.R., Pfister, M., Thomas, B.B., Kashani, A.H., Brant, R., Zhu, D., Clegg, D.O., Hinton, D.R., and Humayun, M.S. (2016). Subretinal implantation of a monolayer of human embryonic stem cell-derived retinal pigment epithelium: a feasibility and safety study in Yucatán minipigs. Graefes Arch. Clin. Exp. Ophthalmol. *254*, 1553–1565.

65. Brant Fernandes, R.A., Koss, M.J., Falabella, P., Stefanini, F.R., Maia, M., Diniz, B., Ribeiro, R., Hu, Y., Hinton, D., Clegg, D.O., et al. (2016). An Innovative Surgical Technique for Subretinal Transplantation of Human Embryonic Stem Cell-Derived Retinal Pigmented Epithelium in Yucatan Mini Pigs: Preliminary Results. Ophthalmic Surg. Lasers Imaging Retina *47*, 342–351.

66. Ilmarinen, T., Hiidenmaa, H., Kööbi, P., Nymark, S., Sorkio, A., Wang, J.H., Stanzel, B.V., Thieltges, F., Alajuuma, P., Oksala, O., et al. (2015). Ultrathin Polyimide Membrane as Cell Carrier for Subretinal Transplantation of Human Embryonic Stem Cell Derived Retinal Pigment Epithelium. PLoS One *10*, e0143669.

67. Kamao, H., Mandai, M., Okamoto, S., Sakai, N., Suga, A., Sugita, S., Kiryu, J., and Takahashi, M. (2014). Characterization of human induced pluripotent stem cell-derived retinal pigment epithelium cell sheets aiming for clinical application. Stem Cell Reports *2*, 205–218.

68. Berglin, L., Gouras, P., Sheng, Y., Lavid, J., Lin, P.K., Cao, H., and Kjeldbye, H. (1997). Tolerance of human fetal retinal pigment epithelium xenografts in monkey retina. Graefes Arch. Clin. Exp. Ophthalmol. *235*, 103–110.

69. Sauvé, Y., Girman, S.V., Wang, S., Keegan, D.J., and Lund, R.D. (2002). Preservation of visual responsiveness in the superior colliculus of RCS rats after retinal pigment epithelium cell transplantation. Neuroscience *114*, 389–401.

70. Thumann, G., Salz, A.K., Walter, P., and Johnen, S. (2009). Preservation of photoreceptors in dystrophic RCS rats following allo- and xenotransplantation of IPE cells. Graefes Arch. Clin. Exp. Ophthalmol. *247*, 363–369.

71. Zhao, C., Boles, N.C., Miller, J.D., Kawola, S., Temple, S., Davis, R.J., and Stern, J.H. (2017). Development of a Refined Protocol for Trans-scleral Subretinal Transplantation of Human Retinal Pigment Epithelial Cells into Rat Eyes. J. Vis. Exp. *126*, e55220.

72. Carr, A.-J.F., Smart, M.J.K., Ramsden, C.M., Powner, M.B., da Cruz, L., and Coffey, P.J. (2013). Development of human embryonic stem cell therapies for age-related macular degeneration. Trends Neurosci. *36*, 385–395.

73. Binder, S., Stolba, U., Krebs, I., Kellner, L., Jahn, C., Feichtinger, H., Povelka, M., Frohner, U., Kruger, A., Hilgers, R.D., and Krugluger, W. (2002). Transplantation of autologous retinal pigment epithelium in eyes with foveal neovascularization resulting from age-related macular degeneration: a pilot study. Am. J. Ophthalmol. *133*, 215–225.

74. Aisenbrey, S., Lafaut, B.A., Szurman, P., Hilgers, R.-D., Esser, P., Walter, P., Bartz-Schmidt, K.U., and Thumann, G. (2006). Iris pigment epithelial translocation in the treatment of exudative macular degeneration: a 3-year follow-up. Arch. Ophthalmol. *124*, 183–188.

75. Falkner-Radler, C.I., Krebs, I., Glittenberg, C., Považay, B., Drexler, W., Graf, A., and Binder, S. (2011). Human retinal pigment epithelium (RPE) transplantation: outcome after autologous RPE-choroid sheet and RPE cell-suspension in a randomised clinical study. Br. J. Ophthalmol. *95*, 370–375.

76. Kashani, A.H., Lebkowski, J.S., Rahhal, F.M., Avery, R.L., Salehi-Had, H., Dang, W., Lin, C.M., Mitra, D., Zhu, D., Thomas, B.B., et al. (2018). A bioengineered retinal pigment epithelial monolayer for advanced, dry age-related macular degeneration. Sci. Transl. Med *10*, eaao4097.

77. da Cruz, L., Fynes, K., Georgiadis, O., Kerby, J., Luo, Y.H., Ahmado, A., Vernon, A., Daniels, J.T., Nommiste, B., Hasan, S.M., et al. (2018). Phase 1 clinical study of an embryonic stem cell-derived retinal pigment epithelium patch in age-related macular degeneration. Nat. Biotechnol. *36*, 328–337.

78. Saishin, Y., Silva, R.L., Saishin, Y., Kachi, S., Aslam, S., Gong, Y.Y., Lai, H., Carrion, M., Harris, B., Hamilton, M., et al. (2005). Periocular gene transfer of pigment epithelium-derived factor inhibits choroidal neovascularization in a human-sized eye. Hum. Gene Ther. *16*, 473–478.

79. Yant, S.R., Meuse, L., Chiu, W., Ivics, Z., Izsvak, Z., and Kay, M.A. (2000). Somatic integration and long-term transgene expression in normal and haemophilic mice using a DNA transposon system. Nat. Genet. *25*, 35–41.

80. Rasmussen, H., Chu, K.W., Campochiaro, P., Gehlbach, P.L., Haller, J.A., Handa, J.T., Nguyen, Q.D., and Sung, J.U. (2001). Clinical protocol. An open-label, phase I, single administration, dose-escalation study of ADGVPEDF.11D (ADPEDF) in neovascular age-related macular degeneration (AMD). Hum. Gene Ther. *12*, 2029–2032.

81. Mori, K., Gehlbach, P., Yamamoto, S., Duh, E., Zack, D.J., Li, Q., Berns, K.I., Raisler, B.J., Hauswirth, W.W., and Campochiaro, P.A. (2002). AAV-mediated gene transfer of pigment epithelium-derived factor inhibits choroidal neovascularization. Invest. Ophthalmol. Vis. Sci. *43*, 1994–2000.

82. Kropp, M., Harmening, N., Bascuas, T., Sealy, G., Conti, A., Johnen, S., Izsvák, Z., Marie, C., Scherman, D., Ronchetti, M., Aranda, P., van den Berg, J., and Thumann, G. (2018). GMP-grade production of tIPE, a cell-based gene therapy product to treat neovascular age-related macular degeneration (nvAMD) developed in the TargetAMD project. Human Gene Therapy *27*, A69.

83. Becerra, S.P., Fariss, R.N., Wu, Y.Q., Montuenga, L.M., Wong, P., and Pfeffer, B.A. (2004). Pigment epithelium-derived factor in the monkey retinal pigment epithelium and interphotoreceptor matrix: apical secretion and distribution. Exp. Eye Res. *78*, 223–234.

84. Thumann, G. (2001). Development and cellular functions of the iris pigment epithelium. Surv. Ophthalmol. *45*, 345–354.

85. Semkova, I., Kreppel, F., Welsandt, G., Luther, T., Kozlowski, J., Janicki, H., Kochanek, S., and Schraermeyer, U. (2002). Autologous transplantation of genetically modified iris pigment epithelial cells: a promising concept for the treatment of age-related macular degeneration and other disorders of the eye. Proc. Natl. Acad. Sci. USA *99*, 13090–13095.

86. Kociok, N., Heppekausen, H., Schraermeyer, U., Esser, P., Thumann, G., Grisanti, S., and Heimann, K. (1998). The mRNA expression of cytokines and their receptors in cultured iris pigment epithelial cells: a comparison with retinal pigment epithelial cells. Exp. Eye Res. *67*, 237–250.

87. Thumann, G., Aisenbrey, S., Schraermeyer, U., Lafaut, B., Esser, P., Walter, P., and Bartz-Schmidt, K.U. (2000). Transplantation of autologous iris pigment epithelium after removal of choroidal neovascular membranes. Arch. Ophthalmol. *118*, 1350–1355.

88. Lappas, A., Weinberger, A.W., Foerster, A.M., Kube, T., Rezai, K.A., and Kirchhof, B. (2000). Iris pigment epithelial cell translocation in exudative age-related macular degeneration. A pilot study in patients. Graefes Arch. Clin. Exp. Ophthalmol. *238*, 631–641.

89. Yasuda, K., Okada, T.S., Eguchi, G., and Hayashi, M. (1978). A demonstration of a switch of cell type in human fetal eye tissues in vitro: pigmented cells of the iris or the retina can transdifferentiate into lens. Exp. Eye Res *26*, 591–595.

90. Okada, T.S. (1980). Cellular metaplasia or transdifferentiation as a model for retinal cell differentiation. Curr. Top. Dev. Biol. *16*, 349–380.

91. Okada, T.S. (1983). Recent progress in studies of the transdifferentiation of eye tissue in vitro. Cell Differ. *13*, 177–183.

92. Wu, Y., Han, F., Quan, Y., Jiang, W., Zhang, H., and Luo, T. (2016). Comparison of peripheral iridectomy methods for posterior chamber phakic intraocular lens implantation in patients with brown irides. BMC Ophthalmol. *16*, 51.

93. Hardee, C.L., Arévalo-Soliz, L.M., Hornstein, B.D., and Zechiedrich, L. (2017). Advances in Non-Viral DNA Vectors for Gene Therapy. Genes (Basel) *8*, 65.

94. Cattoglio, C., Pellin, D., Rizzi, E., Maruggi, G., Corti, G., Miselli, F., Sartori, D., Guffanti, A., Di Serio, C., Ambrosi, A., et al. (2010). High-definition mapping of retroviral integration sites identifies active regulatory elements in human multipotent hematopoietic progenitors. Blood *116*, 5507–5517.

95. Cavazza, A., Moiani, A., and Mavilio, F. (2013). Mechanisms of retroviral integration and mutagenesis. Hum. Gene Ther. *24*, 119–131.

96. Cicalese, M.P., and Aiuti, A. (2015). Clinical applications of gene therapy for primary immunodeficiencies. Hum. Gene Ther. *26*, 210–219.

97. Schatz, H. (1978). Sloughing of skin following fluorescein extravasation. Ann. Ophthalmol. *10*, 625.

98. Fernandez-Robredo, P., Recalde, S., Moreno-Orduña, M., García-García, L., Zarranz-Ventura, J., and García-Layana, A. (2013). Azithromycin reduces inflammation in a rat model of acute conjunctivitis. Mol. Vis. *19*, 153–165.

99. Langmead, B., Trapnell, C., Pop, M., and Salzberg, S.L. (2009). Ultrafast and memory-efficient alignment of short DNA sequences to the human genome. Genome Biol. *10*, R25.

100. Sarver, A.L., Erdman, J., Starr, T., Largaespada, D.A., and Silverstein, K.A.T. (2012). TAPDANCE: an automated tool to identify and annotate transposon insertion CISs and associations between CISs from next generation sequence data. BMC Bioinformatics *13*, 154.

101. R Development Core Team. (2008). R: A language and environment for statistical computing (R Foundation for Statistical Computing).

102. Akalin, A., Franke, V., Vlahoviček, K., Mason, C.E., and Schübeler, D. (2015). Genomation: a toolkit to summarize, annotate and visualize genomic intervals. Bioinformatics *31*, 1127–1129.

103. Kozhevnikova, O.S., Korbolina, E.E., Ershov, N.I., and Kolosova, N.G. (2013). Rat retinal transcriptome: effects of aging and AMD-like retinopathy. Cell Cycle *12*, 1745–1761.